Pergamon

Journal of Structural Geology, Vol. 17, No. 2, pp. 183 to 199, 1995

0191-8141/95 $9.50 + 0.00

0191-8141(94)E0043-X

The evolution of crustal deformation in an oceanic extensional environment

EDDIE MCALLISTER and JOHNSON CANN

Department of Earth Sciences, University of Leeds, Leeds LS2 9JT, U.K.

and

SARA SPENCER

Department of Geology, The American University of Beirut, Beirut, Lebanon

(*Received* 27 *September* 1993; *accepted in revised form* 18 *March* 1994)

Abstract—Fault statistics collected along the slow-spreading Reykjanes Ridge are used to investigate its complex tectonic evolution. The Reykjanes Ridge is oriented oblique to the spreading direction and is located close to the Iceland hotspot. A wide distribution in fault strike and fault throw occurs across the axis of the Reykjanes Ridge, with a sharp change in mean strike and mean throw occurring at the edge of the axial zone. Within the axial zone there is no significant change in the distribution of faults with increasing distance from Iceland; proximity to the hotspot does not influence the detailed tectonics near the axis. We infer that the fault development within the axial zone is controlled by the plate tectonic generated regional stress field.

Outside the axial zone the faults strike oblique to the spreading normal direction. This change in fault strike, coupled with the lack of any evidence for strike-slip movement, suggests that these faults develop as a passive response to the thermal evolution of the lithosphere.

Our results indicate that at a slow-spreading ridge the crust is deformed by two stress fields, one responsible for the fault formation within the axial zone, the other for the faults which bound the axial zone.

INTRODUCTION

Located between Iceland in the northeast and the Charlie Gibbs Fracture Zone in the southwest, the Reykjanes Ridge is the northern extension of the Mid-Atlantic Ridge (Fig. 1). The Reykjanes Ridge has several characteristics that set it apart from other ridges. It spreads obliquely, so that while the spreading direction is 099° (Minster & Jordan 1978), the ridge trend is 036°, at 27° to the spreading normal (009°) direction. The ridge spreads slowly, with a half spreading rate of 10 mm a^{-1} (Minster & Jordan 1978, Talwani *et al.*, 1971, Vogt & Avery 1974), yet the bathymetric morphology is more akin to that of a fast spreading ridge. In the region close to Iceland, the axis of the ridge is marked by a smooth median high as opposed to a median valley. With increasing distance south-west from Iceland three major changes in ridge morphology occur. There is a gradual transition from a well-developed axial high to a median valley with the same depth as the Mid-Atlantic Ridge farther south. The width of the axial zone, which we define to be the zone between the innermost boundary faults on either side of the axis, narrows and the depth to the crest of the ridge increases from sea level at the Reykjanes Peninsula in Iceland at 63.8°N to normal oceanic depths at the Bight Fracture Zone at 57°N. Associated with these changes is an increase in the topographic roughness on the flanks of the ridge. These changes in morphology are correlated with changes in magma geochemistry, from a plume dominated chemistry near Iceland to a MORB chemistry at about the point where the axial high gives way to a median valley (Schilling 1975). Coupled geochemical and morphological studies provide a powerful tool for mapping the influence of the Icelandic hotspot upon the ridge system.

Throughout the 800 km length of the Reykjanes Ridge there is only one fracture zone, the Bight Fracture Zone at 57°N. Except at this latitude, magnetic anomalies are continuous and unbroken by offsets, and run parallel to the spreading axis (Vogt & Avery 1974) back to anomaly 6 (20 Ma ago). Bathymetric maps show that out to anomaly 6 the topography is ridge parallel. Older magnetic anomalies show that the ridge was broken into a conventional staircase of ridge segments normal to the spreading direction offset by fracture zones (Vogt & Avery 1974). Even earlier, before anomaly 18 time (45 Ma ago), the magnetic anomaly pattern of the ridge was similar to its present state. At present there is a small-scale segmentation of the ridge axis, which does not affect magnetic anomalies or regional topography and which is characterized by a series of en échelon axial volcanic ridges (AVRs) described by Shih *et al.* (1978), Jacoby (1980) at 62°N, Searle & Laughton (1981) between 58° and 61°N and more recently by Parson *et al.* (1993) between 58° and 62°. These en échelon AVRs are oriented at 014° and have been recognized only within the 8–15 km wide axial zone. Successive AVRs overlap each other by up to 50% of their length. The edge of the

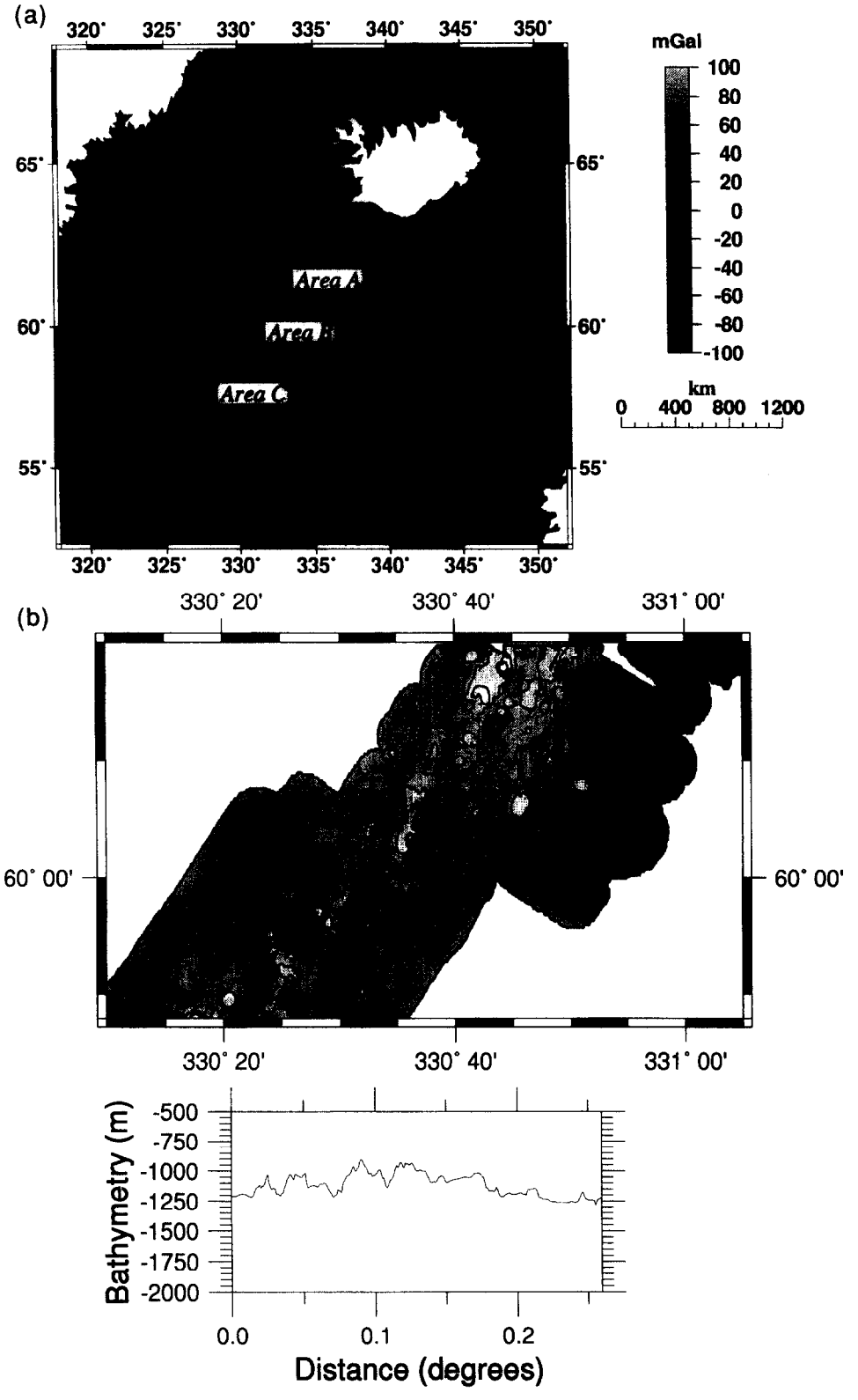

Fig. 1. (a) Free-air gravity map of the survey area. The shaded regions represent the three areas surveyed during EW9008. Area A has only a bathymetric survey while areas B and C have detailed sidescan sonar as well (b) Bathymetric map and cross-section of area B, the contour interval is 50 m. The cross-section is taken along the 60°N line of latitude, and has a vertical exaggeration of ×10. (c) Bathymetric map and cross-section of area C, the contour interval is 50 m. The cross-section is taken along the 58°N line of latitude, and has a vertical exaggeration of ×10.

axial zone is defined by inward facing faults striking 028° sub-parallel to the ridge axis and therefore oblique to the spreading direction. The first ridge parallel faults appear at a mean distance of 4.7 km from the ridge axis and the topography of the ridge flanks is dominated by the parallel traces of major faults spaced on average 9.4 km apart (Laughton *et al.* 1979). The Reykjanes Peninsula, the onland extension of the Reykjanes Ridge, has right stepping en échelon rifts similar to the volcanic ridges identified along the spreading ridge, except that there

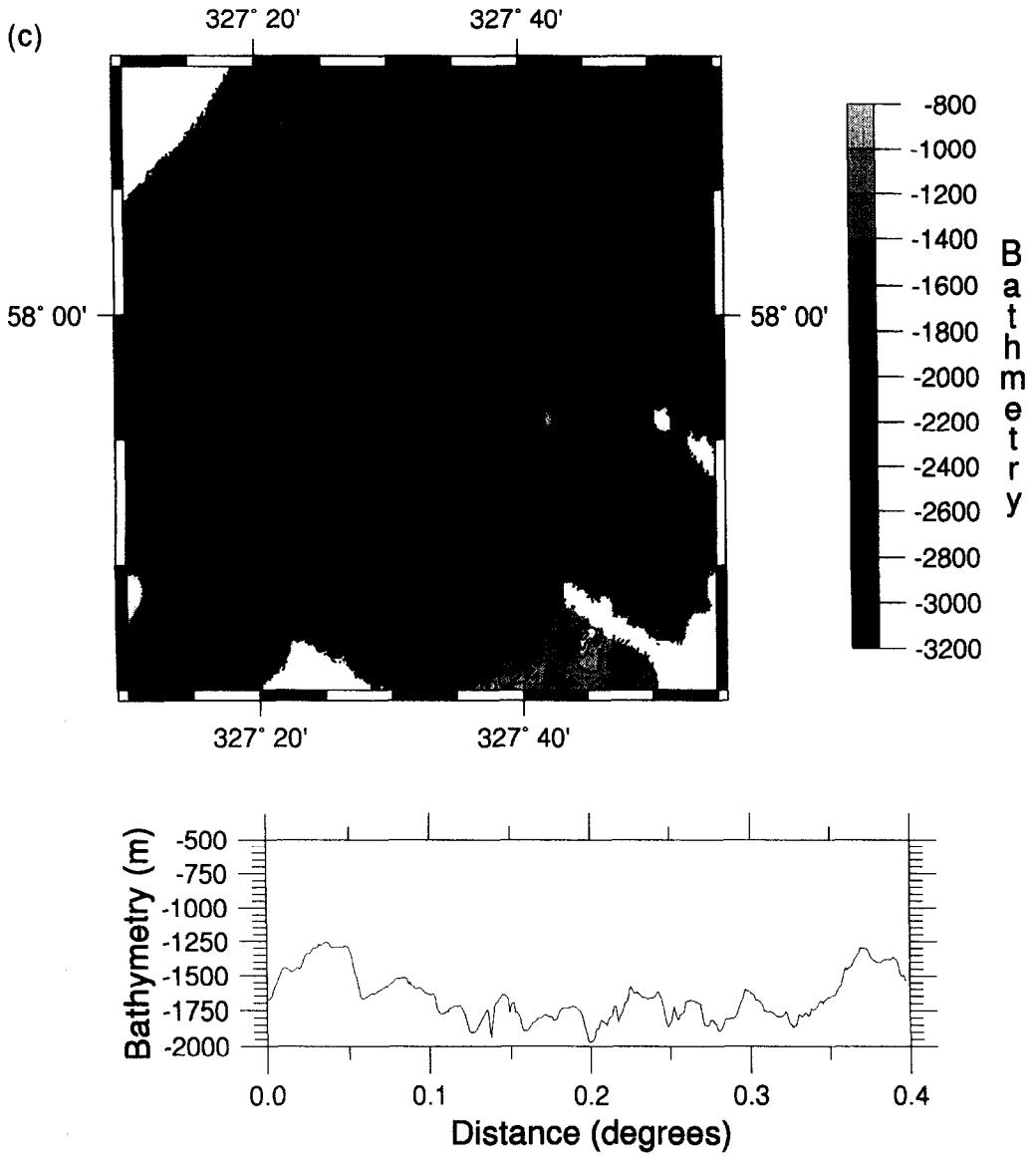

Fig. 1. (*Continued*)

the strike of faults and volcanic systems is rotated clockwise to become subparallel with the axis of the Reykjanes Ridge (Gudmundsson 1987).

The Reykjanes Ridge is often considered to be anomalous because of its unusual morphological features and because of its proximity to Iceland. But it clearly forms part of a spectrum of types of spreading centres, and its features require explanation. In addition, its unusual characteristics may allow tectonic processes to be better understood than in more typical spreading centres. In particular the oblique angle between spreading normal and ridge axis strike allows for the disentangling of tectonic processes related to crustal accretion from those related to the construction of the bounding faults of the median valley.

The aim of this paper is to present new and detailed fault data which spans the volcanic axis and out to beyond the median valley. The data are used to address problems concerning the generation of fine-scale tectonics within the median valley and the creation of the faults which bound the median valley. We used records from a new high resolution side-looking sonar to identify faults. These faults are then measured for strike and displacement relative to the axis. We present a model of a changing stress field with distance from the axis, with a sharp transition between deformation within the zone of crustal accretion and tectonic deformation associated with the creation of the median valley bounding faults.

PREVIOUS WORK

Laughton *et al.* (1979) and Searle & Laughton (1981) provide the most detailed observations made of the Reykjanes Ridge. They noted that the axial zone is segmented into en échelon ridges which they hypothesized are single magmatic segments. Their study also highlighted the obliquity between the AVRs (014°) and the median valley bounding faults (028°), showed that faults in the crustal mountains tended to throw down towards the median valley and demonstrated that there is a change in morphology from a 'fast-spreading' mor-

phology (non-rifted) to a 'slow-spreading' morphology (rifted) along the ridge axis away from Iceland.

Lobate reflections from within the axial zone led Laughton *et al.* (1979) and Searle & Laughton (1981) to the hypotheses that the AVRs had accumulated from lavas erupted from fissures. Searle & Laughton further postulated that the AVRs and the minor faulting and fissuring were generated by a 'horizontal tension imposed by the separation of the plates at the ridge axis'. They envisaged episodic activity of the overlapping AVRs with only one being active at any one time.

The recognition of the rift to non-rift transition (Searle & Laughton 1981) was emphasized by the variation in displacement of the axial zone bounding faults with progressive distance from Iceland. The bounding faults show an increase from a mean displacement of 96 m in the northeast to 275 m in the south-west of their survey area. A similar variation orthogonal to the ridge axis was not observed. Such a marked change across the rift/non-rift transition (which occurs at approximately 60°N) has also been shown in the gravity data (Hwang *et al.* in press) and geochemical data (Schilling 1975). Thus the transition is an important tectonic and magmatic feature of the increasing distance from the Icelandic hotspot.

DATA COLLECTION AND ANALYSIS

The aim of the survey was to examine the detailed morphology of selected areas of the Reykjanes Ridge between 57° 35′N and 62° 05′N using echo sounder (12 and 3.5 kHz), a multibeam swath mapper (Hydrosweep) and a deep-towed sidescan sonar (TOBI). The sidescan has a total swath width of 6 km. The resolution of the sonar is dependent on range; close in to the vehicle track the insonified footprint has an along-track dimension of 7 m and an across-track dimension of 4 m. At far range these dimensions change to 42 m by 2 m, respectively (Flewellen *et al.* 1993).

EW9008 surveyed three areas of the Reykjanes Ridge (Fig. 1), though only two areas were mapped by both TOBI and Hydrosweep. In order to facilitate correlation between this paper and Parson *et al.* (1993) we have adopted the same names for the survey areas, namely areas A, B and C. We will focus on areas B and C. Area B lies between 59°56′ & 60°40′N and 28°28′ & 29°35′W, while area C lies between 57°35′ & 58°25′N and 31°47′ & 33°04′W (Figs. 1b & c). The two areas lie north and south, respectively, of the transition from an axial high to an axial valley (the non-rift to rift transition). Two sources of data exist for the axial zone, deep-towed sidescan sonar images and the multibeam swath map. Figures 2 and 3 show comparisons between sidescan sonar images and the multibeam swath map for areas B and C, respectively. Beyond the first boundary faults the multibeam map is the sole data source for the fault statistics.

Fault interpretation was based on comparisons between Hydrosweep bathymetric maps and TOBI sidescan images. Because the resolution of the Hydrosweep multibeam system is lower than that of the TOBI sidescan system, only faults with a throw greater than 25 m are detectable on the multibeam maps. On the Hydrosweep maps, faults are identified by closely spaced contours which are linearly persistent. The larger faults can be identified on both data sets, although each image gives a different type of information. From the Hydrosweep maps the height of the fault scarp, taken to be the fault throw, and the gradient of the topographic slope can be measured, while the TOBI images reveal details of the fault morphology and the materials that make up the fault scarps. Such joint interpretation is only possible in the axial zone where both types of data are available. Outside that zone, interpretation must rely on Hydrosweep data alone, drawing upon relations between scarps and topography seen in the axial zone. Estimation of fault dip from topography on the bathymetry maps is a very unreliable indicator of the true dip of the fault scarp. The Hydrosweep system may introduce artifacts in the regions of steep slope, the bathymetry maps are gridded at 100 m intervals, such that the apparent dip is an averaged slope, and major fault scarps are invariably covered by a considerable amount of talus, reducing the topographic gradient. We have therefore chosen not to measure the gradient of fault-related slopes.

In order to investigate any relationship between fault strike and distance from the volcanic axis, and because of the complex interaction of faults which make it difficult confidently to pin point a single fault trace, we subdivided all faults identified on the TOBI images into 500 m segments, referred to in the text as 'fault segments'. We then measured the strike, distance and displacement (where the faults were detected by Hydrosweep) from the spreading axis of these fault segments. The displacement on a fault segment was calculated by assuming: (1) that the exposed scarp represents the total throw of the fault; and (2) that sediment thickness is much smaller than the fault scarp height, and does not affect the fault profile.

FAULT PATTERNS

The bathymetry maps of area B lie within the axial zone as defined by Searle & Laughton (1981) and as such display very few indicators of where the edge of the axial zone lies. The shallowest regions of the axial zone are located on the AVRs, and the topography generally deepens on either side to the edge of the available data (like a fast spreading ridge) (Figs. 1b & c). Superimposed on this regional bathymetry are small circular features which are found throughout the area; we interpret these features as small volcanoes based on their similarity to features in other areas of slow spreading ridges (e.g. Smith & Cann 1992). Thus, while area B has a gross bathymetry similar to that of a fast spreading ridge, its detailed near-axis bathymetry is more akin to that of a slow-spreading ridge.

Area C contrasts strongly with that of area B; the axial

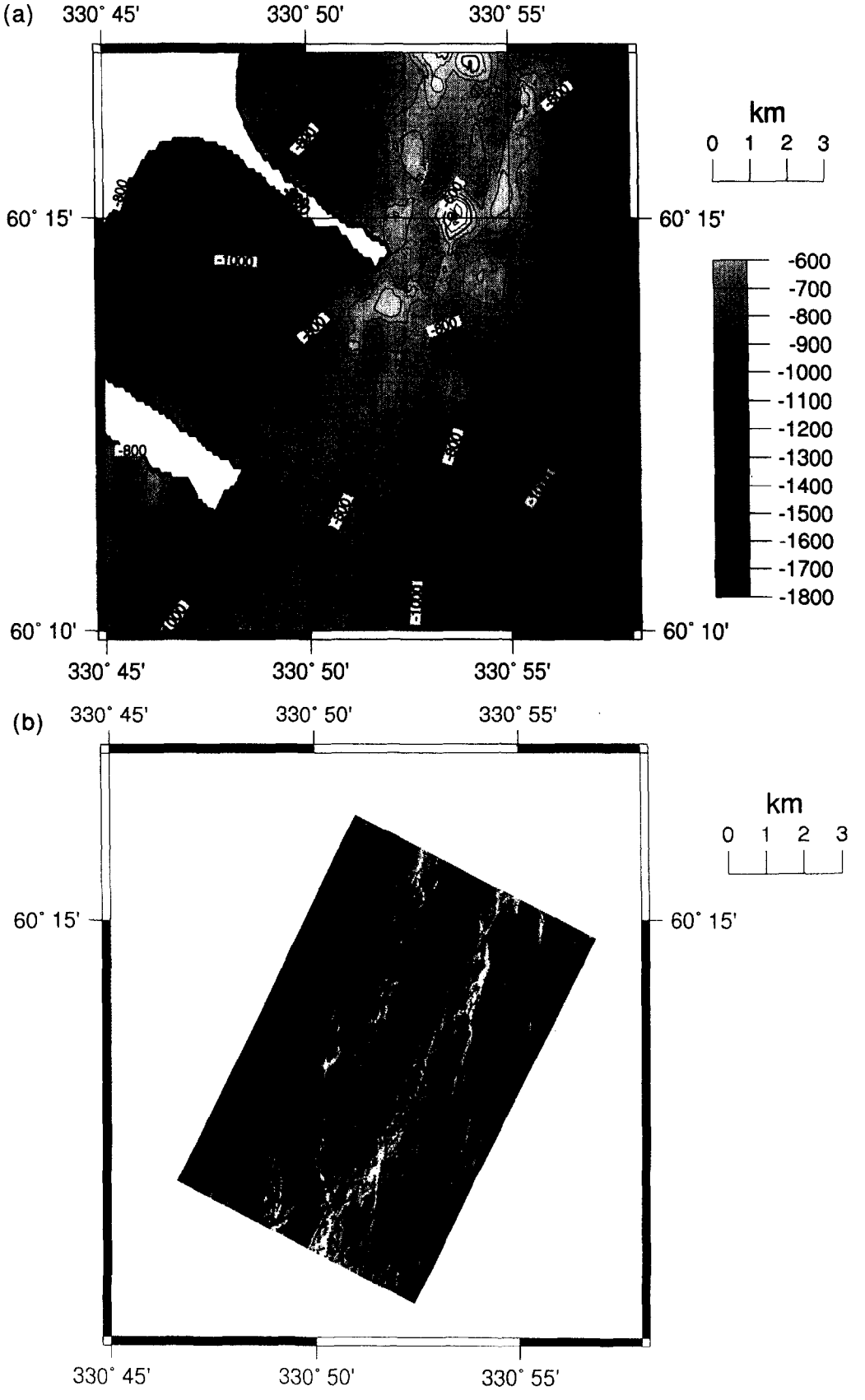

Fig. 2. Hydrosweep swath multibeam plot (a) and sidescan sonar image (b) for part of area B, the contour interval for the plot is 25 m. The plot locates the position of the sidescan image. This image is a single swath of sidescan, with the dark scalloped line in the centre representing the track of the vehicle. The swath width is 3 km on both sides with a near field resolution of 2–5 m. This image was manually mosaiced to correct for variations in ship's speed and slack in the towing cable. The bright (white) zones cutting obliquely across the image are interpreted as small fault scarps. Note the lack of any evidence for these faults on the bathymetric plot. Circular features of varying scales (10's–100's m) are interpreted as small volcanoes and hummocky volcanic terrain.

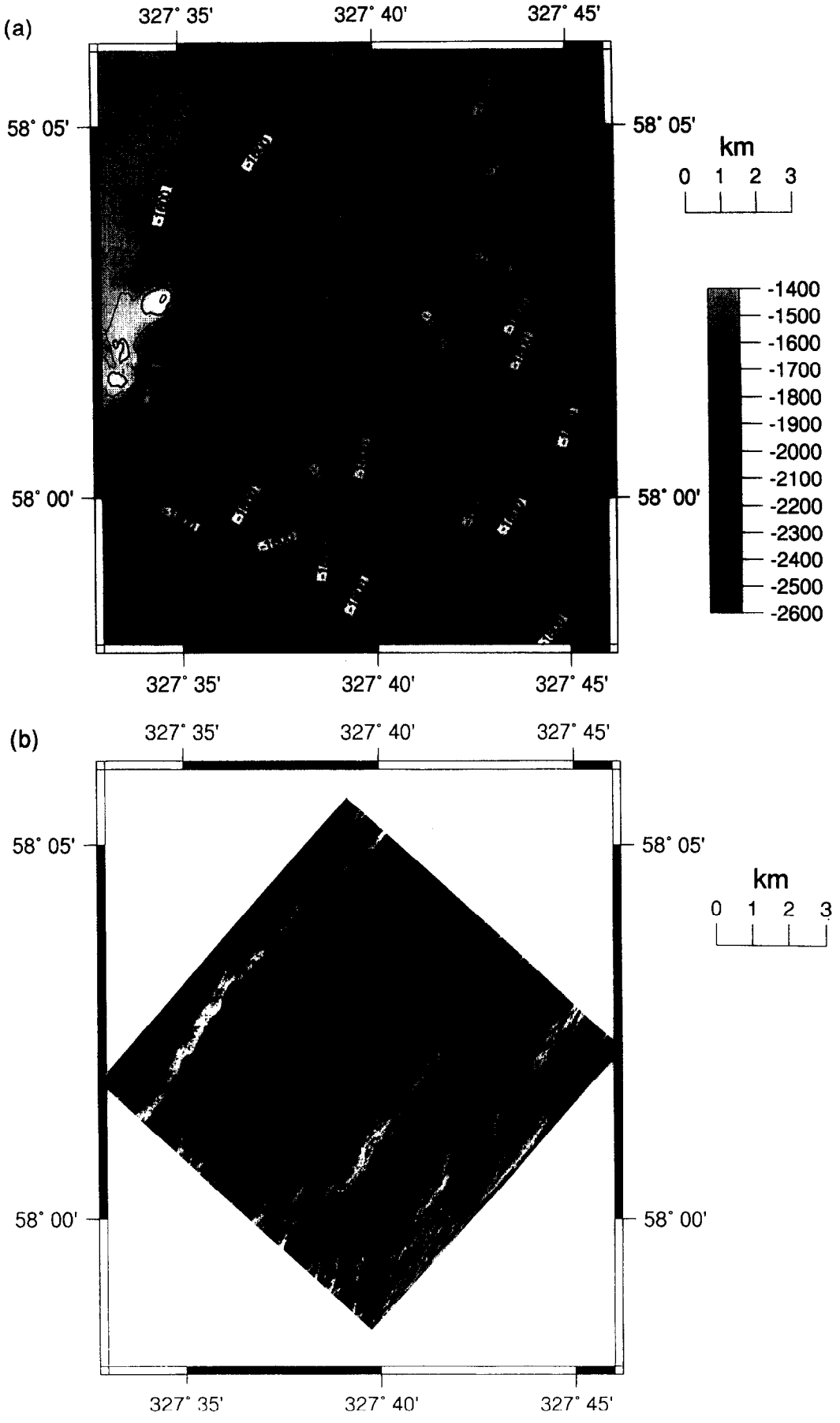
(a)
327° 35'
327° 40'
327° 45'
58° 05'
58° 00'
km
0 1 2 3
-1400
-1500
-1600
-1700
-1800
-1900
-2000
-2100
-2200
-2300
-2400
-2500
-2600
(b)
327° 35'
327° 40'
327° 45'
58° 05'
58° 00'
km
0 1 2 3

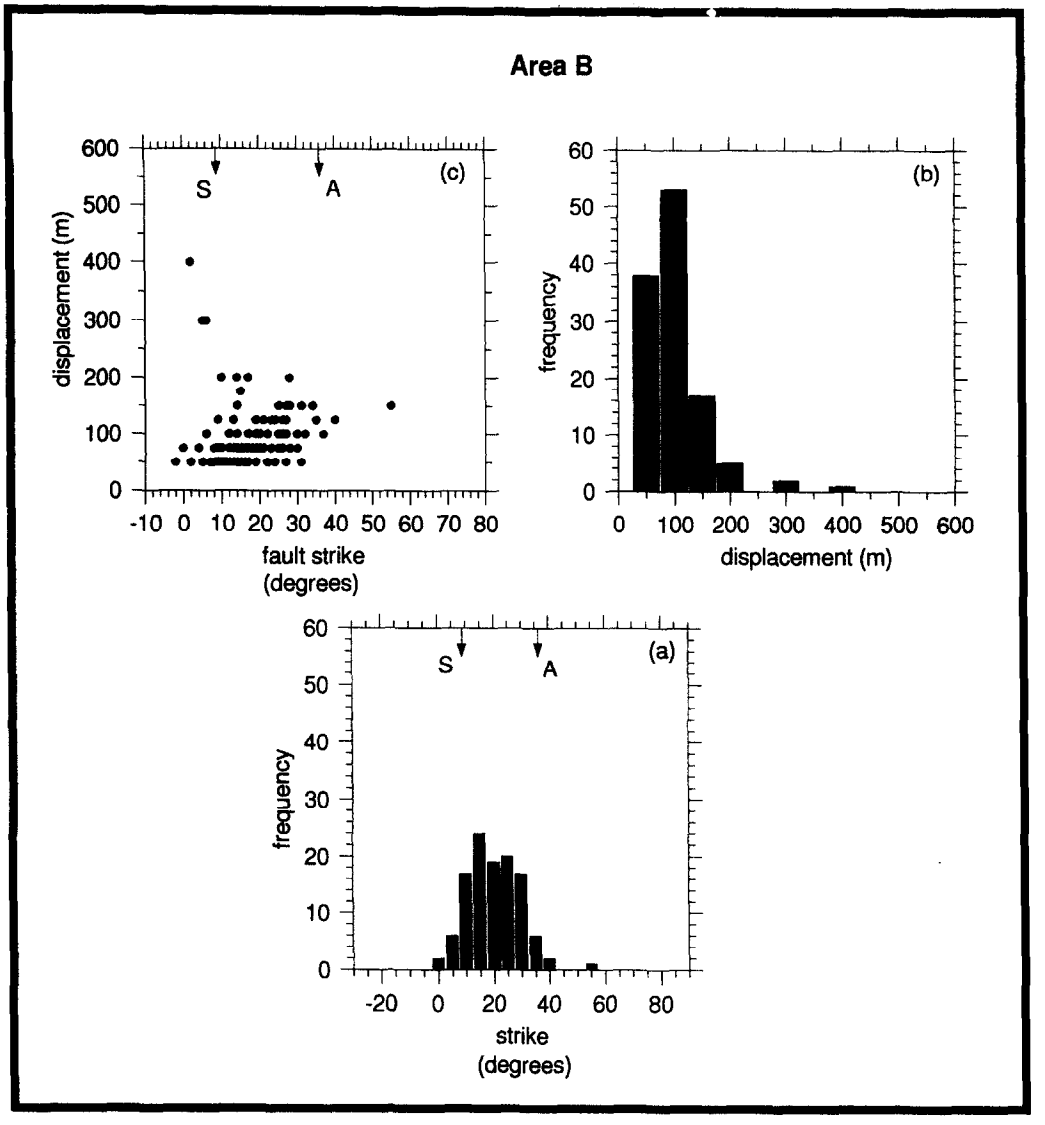

Fig. 4. Fault statistics from Hydrosweep maps of area B. Plots show (a) the variations of strike of the fault segments relative to displacement, (b) frequency histograms of fault segments displacements, and (c) fault segment strike for area B. *S* is the spreading normal direction and *A* the axis parallel direction derived.

zone is clearly defined by faults trending parallel to the strike of the ridge. The depth to the ocean floor increases away from the axis until it is checked at the boundary faults where the relief increases. Thus in less than 200 km along strike the axial zone of the ridge changes from a smooth axial high to a rougher, fault-bounded median valley.

Area B

Bathymetry. The Hydrosweep maps for the axial zone of area B are dominated by circular shaped volcanic constructions, hundreds to thousands of metres across, with few areas containing contour patterns which satisfy our criteria for a fault. In area B there is no tectonic lineament on the bathymetric maps identifying the edges of the axial zone. The morphology changes with distance from the spreading axis from en échelon axial volcanic ridges, with numerous circular features of various sizes, to a flanking smoother surface interrupted only by large circular highs (1000–2000 m across). The ocean floor gently increases in depth away from the axis, with few signs of the creation of topography away from axis. All faults identified from Hydrosweep maps are shorter than 4000 m.

The mean strike of the fault segments (Fig. 4a) is 020° and the average throw is less than 100 m (Fig. 4b). Only seven measured segments show throws ≥200 m. A

Fig. 3. A comparison between the multibeam swath map (a) and sidescan sonar image (b) for area C. As Fig. 2 except that the sidescan image is made up of two partially overlapping swaths. Note for this figure the insonification direction changes across the vehicle track line, marked by a continuous black zone with regularly spaced white dashes, and across the join between the two images, which is a vertical join in the middle of the image. The large bright zone of backscatter to the left of the image represents the bounding fault of the median valley in this area. This fault is also recorded on the bathymetric plot. The sidescan image relays greater information about the fine scale texture and geometry of this fault scarp. The sidescan image covers an area of 10 km by 10 km.

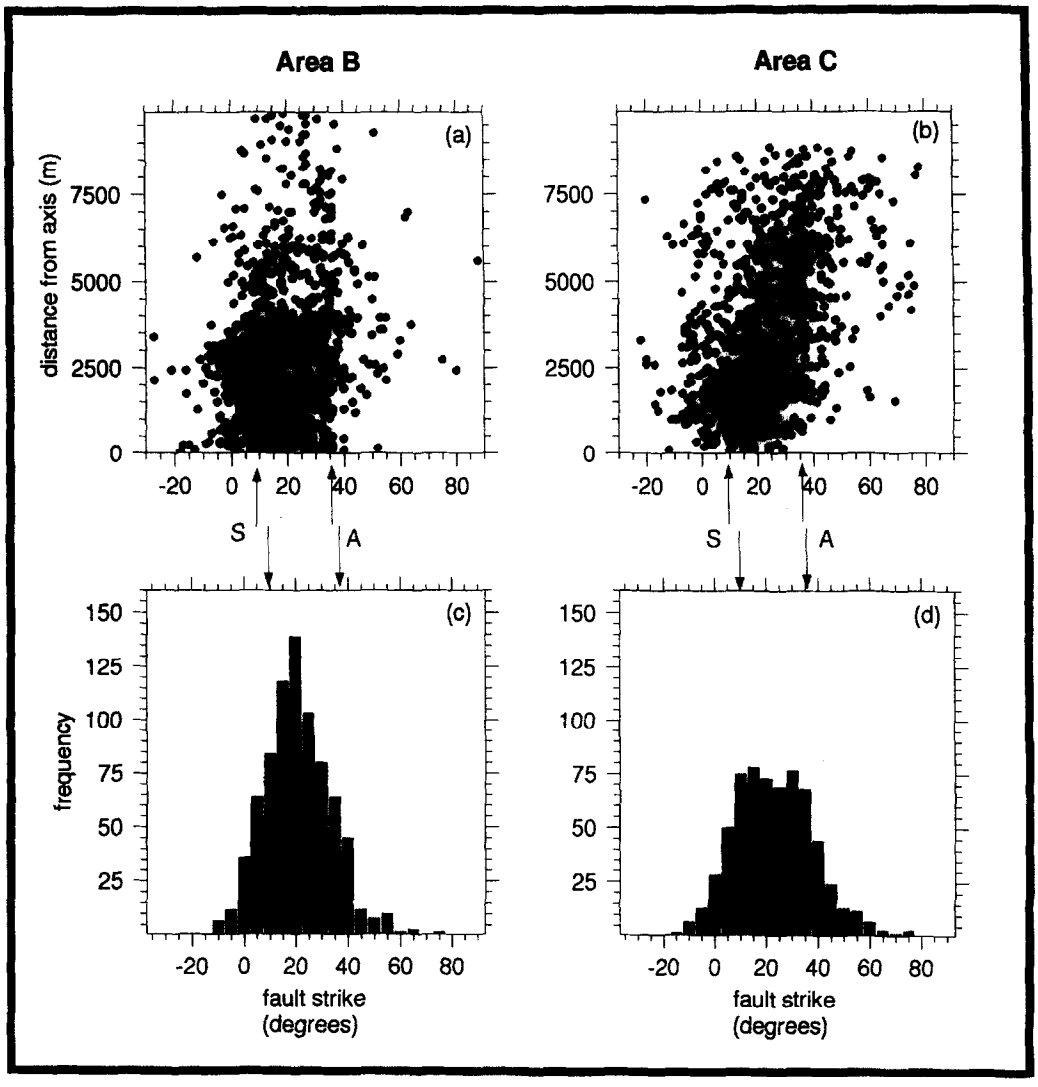

Fig. 5. Histograms and scattergrams derived from TOBI side-scan images depicting the range in fault orientations and distance from the axis for areas B and C. (a) & (b) show the variation in strike with distance from the ridge axis, for areas B and C, respectively. (c) & (d) show histograms of fault strike for the same areas. The number of data points are 969 and 1024 for areas B and C, respectively. *S* is the spreading normal direction and *A* the axis parallel direction derived.

relationship exists between the strike of the fault segments and their displacement, indicating that faults with a large displacement are more likely to be oriented close to axis parallel than those faults with a smaller displacement (Fig. 4b). The mean strikes of the fault segments with throws less then 100 m and between 100 and 200 m are 017° and 025°, respectively. A *t*-test on these two groups allows the hypothesis that they are both drawn from the same population to be rejected at the 95% level. Thus faults with a small displacement are more likely to strike AVR parallel, while those with a larger displacement will strike between AVR and axis parallel.

Sidescan. While the bathymetry of area B displays only sparse tectonic indicators, the sidescan images show abundant fine-scale sinuous and linear zones of strong backscatter. We interpret the linear zones to represent faults with throws of less than 25 m.

There is a wide distribution on the sidescan records in fault segment strike within area B from 342° to 088°, with a reduction in the number of recorded fault segments with increased distance from the axis (Fig. 5). In order to investigate any spatial change in the characteristics of the fault segments with distance from the axis the data were subdivided into four zones of different distances from the axis (0–2 km, 2–4 km, 4–6 km and 6–10 km). A *t*-test was made comparing the orientation data from the four zones. The hypothesis that the orientation data for successive pairs of zones are drawn from the same population is rejected a the 95% confidence level when comparing the 0–2 km zone with the 2–4 km zone, and the 2–4 km zone with the 4–6 km zone, but is not rejected when comparing the 4–6 km zone with the 6–10 km zone (see Table 1). Figures 6(a)–(d) display the orientation distribution of the fault segments associated with the different zones, while Table 1 lists the statistics for the fault segments. In Fig. 6 all the fault statistics data have been normalized to give fault segment density per km^2 of the area surveyed. This allows quantitative comparison between different parts of the same survey area. Normalization is achieved by calculating within a given zone the area covered by the sidescan and dividing that into the number of fault segments found within that zone. From the normalized data, difference diagrams can be

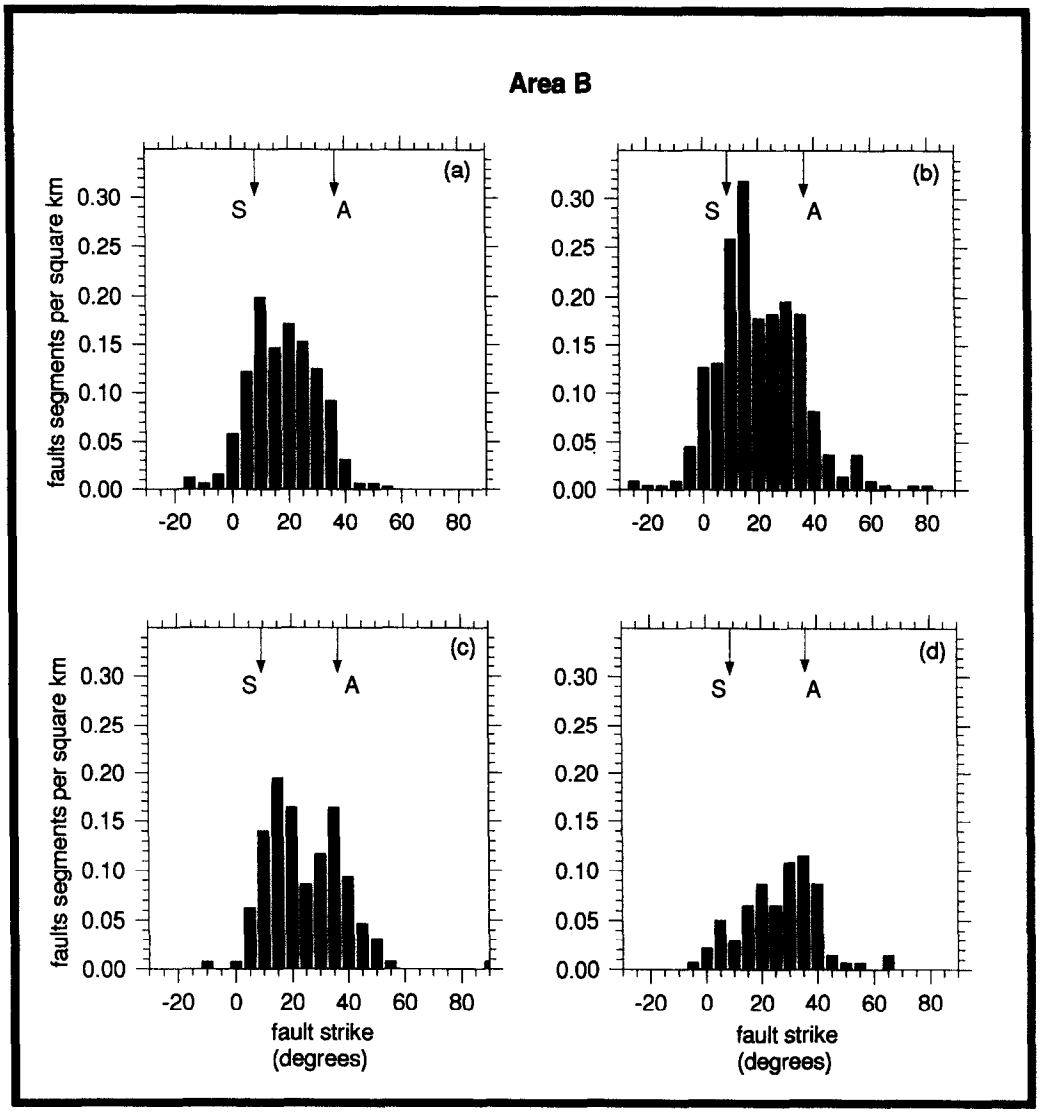

Fig. 6. Frequency diagrams derived from TOBI side-scan images showing the orientation distribution of the density of fault segments at incremental distances from the axis within area B: (a) 0–2 km; (b) 2–4 km; (c) 4–6 km; (d) 6–10 km. All the data has been normalized according to the percentage coverage of sidescan over the areas. The fault segments were all measured from the sidescan images, with each segment being 500 m in length.

Table 1. Statistics from fault segment data measured form the sidescan images, at incremental distances from the axis, for areas B and C

	Distance (m)	Mean orientation (degrees)	Standard deviation	Number of data points	Density (km^2)
Area B	0–2000	15.92	11.86	375	1.15
	2001–4000	18.11	15.1	404	1.84
	4001–6000	22.79	13.71	145	1.13
	6001–10,000	24.23	13.25	94	0.68
Area C	0–2000	16.46	12.82	300	0.9
	2001–4000	19.48	15.18	244	0.997
	4001–6000	29.58	14.68	224	1.7
	6001–10,000	32.18	18.14	196	1.13

calculated (Fig. 7). These show the difference in normalized fault segment abundance as a function of fault segment strike between successive zones at increasing distance from the spreading axis. Negative values show a decrease in abundance caused, for example, by faults being buried by lava flows or covered by sediments, while positive values show an increase in fault activity.

Within 2 km of the axis the faults have a mean strike of 016°, sub-parallel to the strike of the AVRs and the spreading normal direction. In the region 2–4 km from the axis there is a slight shift in the mean strike to 018°, but, more dramatically, the density of fault segments has increased by 64%. The sidescan images have no patches within area B that are either highly or sparsely faulted

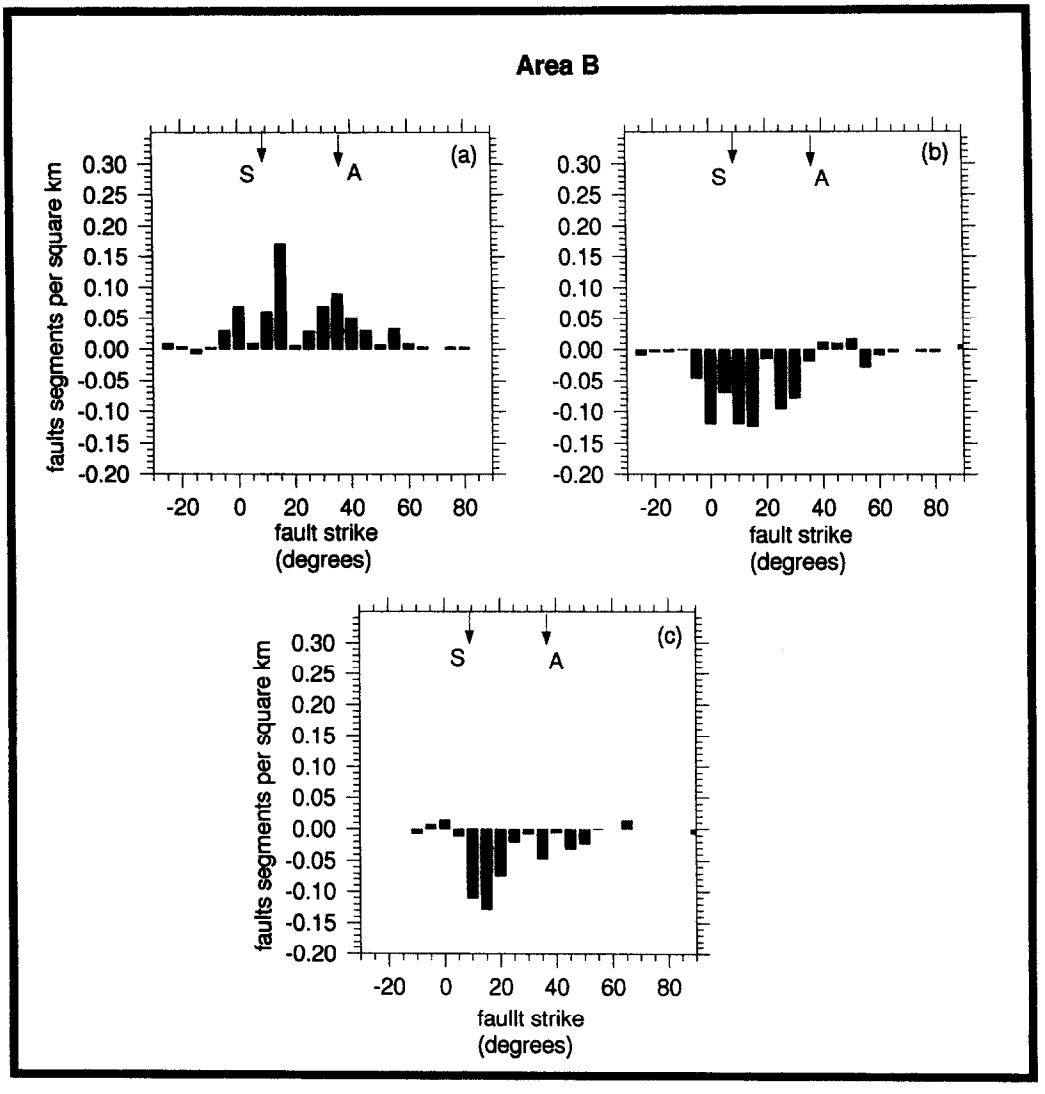

Fig. 7. Histograms of difference between fault segment strikes in adjacent zones for the sidescan data in area B. (a) Difference between Figs. 6(a) & (b), (b) difference between Figs. 6(b) & (c), and difference between Figs. 6(c) & (d).

nor are faults noticeably longer than those found nearer to the axis. Thus the increase in the density of fault segments represents an increase in the number of faults per km^2 over the whole area. A further clockwise change in strike occurs at 4–6 km from the axis where the main strike is 023°, 7° greater than found at the axis. The density of faults is reduced when compared to the previous segment (Fig. 7), and the sidescan images display patches of low backscatter typical of the level found by sediments.

Clearly, with increasing distance from the axis both the strike and the density of faults varies (Fig. 6): within 4 km of the axis there is an overall increase in the density of faults, while outside 4 km the density of the fault segments is reduced (Figs. 6b & c). There is a clockwise rotation in the mean strike with increasing distance from the axis as far as 6 km, but beyond that the rotation ceases.

Area C

Bathymetry. As is the case with area B the Hydrosweep bathymetry shows few faults with throws greater than 50 m occurring within 4 km of the axis. The one section of area B where faults are large enough to register on the bathymetric maps has been described by Owens *et al.* (1991) and was interpreted from gravity and bathymetry data to be a non-transform offset.

In area C the edge of the median valley is clearly defined by bunching contours running parallel to the axis and oblique to the AVR trend. The statistics of the fault segments derived from these fault traces are shown in the histograms of Fig. 8. Ridge axis parallel faults are seen on both the sidescan sonar image and the multibeam swath maps of area C, though it is only the youngest axis-parallel faults, those bounding the axial zone, that are within the area covered by the sidescan sonar. All faults farther from the axis have only been imaged by the multibeam swath mapper. There is no evidence for a systematic increase in fault throw with distance from the axis. We consider that most of the growth of faults seen on bathymetry maps takes place at the site of the first axis-parallel fault. This concurs with the findings of Searle & Laughton (1981).

On the bathymetric maps we identified no faults dipping away from the axis, either in the off-axis zone or

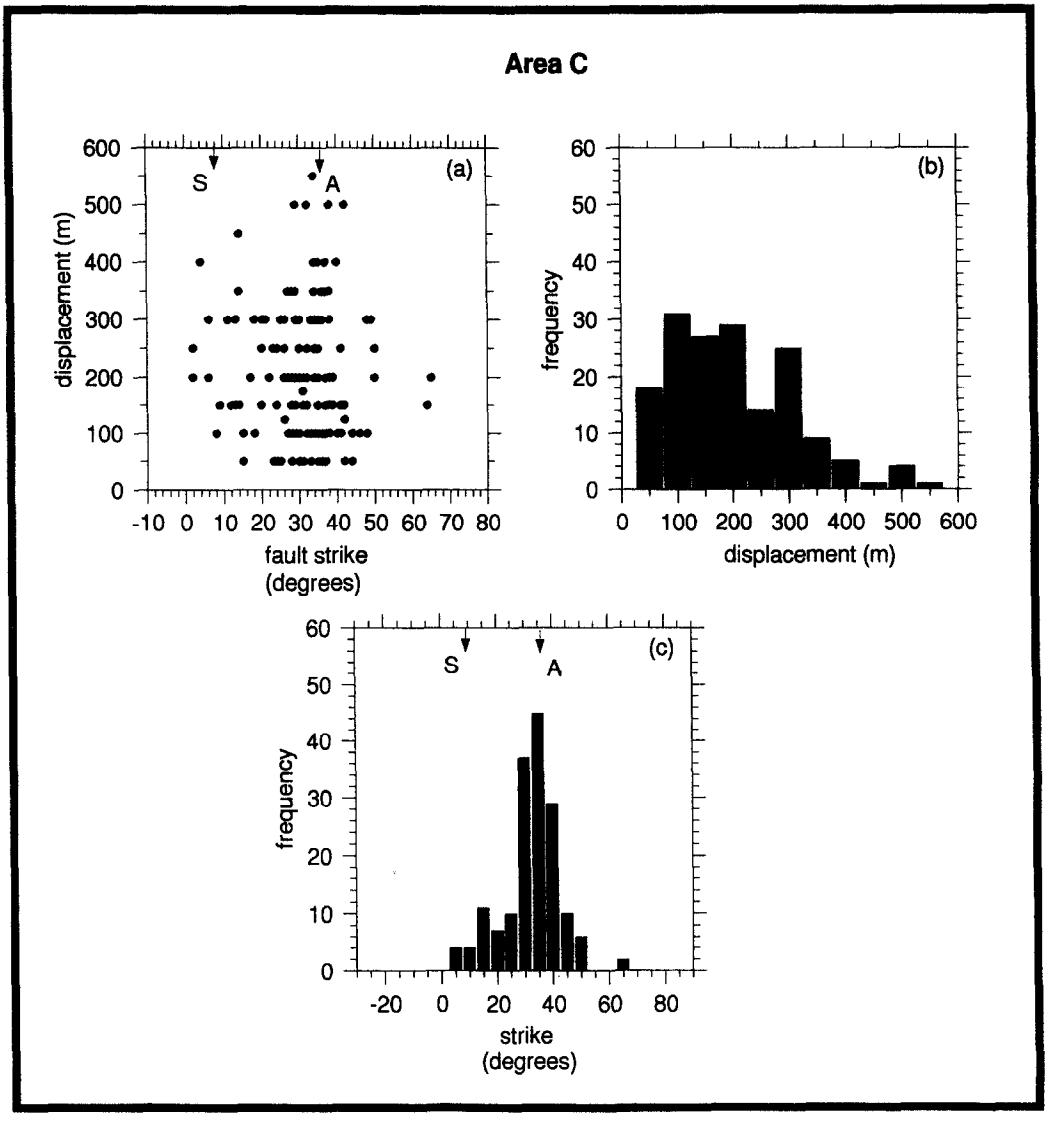

Fig. 8. Fault statistics from Hydrosweep maps of area C. Plots show (a) the variations of strike in the fault segments relative to its displacement, (b) frequency histograms of fault segment displacements, and (c) fault segment strike for area C. *S* is the spreading normal direction and *A* the axis parallel direction.

in the axial zone. There exist areas of steep topography dipping away from the ridge axis, though we do not consider these to be faults for two reasons. No outward throwing major faults were identified on the GLORIA survey of the Reykjanes Ridge (Searle & Laughton 1981). In addition, in our recent survey over off-axis faults on the Mid-Atlantic Ridge further south (between 25° and 30°N) all faults are observed to dip towards the axis. In the Reykjanes Ridge outward dipping surfaces are generally less steep and less linear than the inward dipping surfaces shown by TOBI to be faults.

The dominant slip direction on the fault planes was deduced from the displacement of small volcanic edifices dissected by faults. Only vertical displacements were observed throughout both areas B and C. No significant strike-slip displacement was identified. Dip-slip (normal) faulting is indicated by focal mechanisms in this area (Bergman & Solomon 1990).

A ubiquitous feature of the faults is the presence of a hangingwall depression, with maximum depth coincident with the centre of the fault trace, and the depth to the basin tapering off towards the fault tip (Fig. 9). Such basins have a maximum length parallel to the fault strike of 6000 m, and a maximum depth of 200 m.

The distribution of 500 m fault segments measured from the Hydrosweep maps for area C are shown in Fig. 8. The mean throw is 200 m, with a maximum of 550 m. Unlike in area B there is no obvious variation in fault throw with fault segment strike, with a mean strike of 032°, close to that reported by Searle & Laughton (1981) for the axis parallel faults. A *t*-test comparing the orientation of fault segments with a throw less than 100 m with the orientation of those with a throw greater than 100 m shows no significant difference.

Sidescan. In area C, TOBI sidescan images were obtained of the axial zone, out to and just beyond, the first major bounding fault. Almost all of the faults imaged in area C thus lie within the axial zone. The shape of individual faults within area C is similar to those of area B; faults within the axial zone are sinuous with a slight variation in the width of back-scatter along strike.

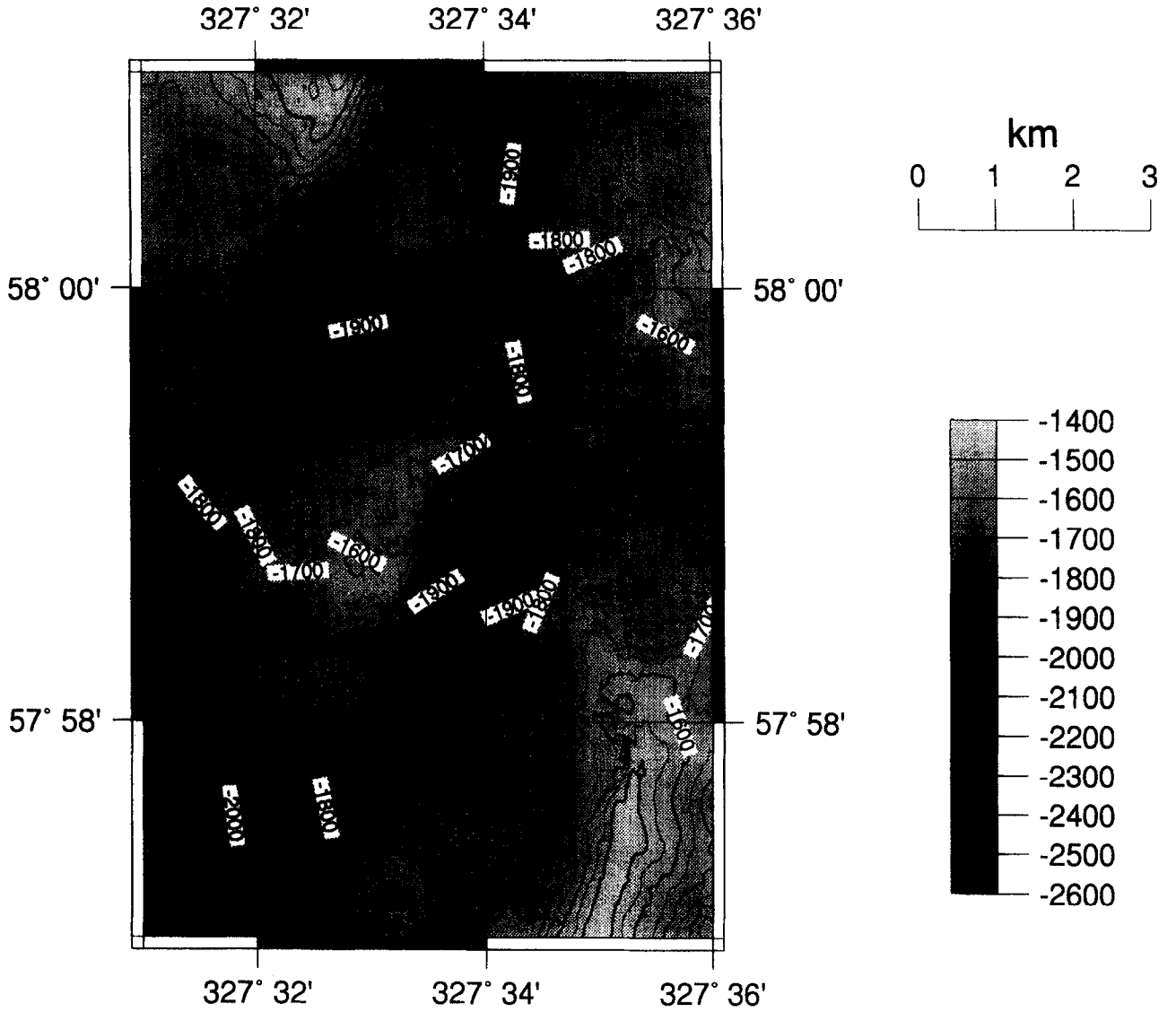

Fig. 9. Hydrosweep map of a single fault with a footwall high, a hangingwall basin and a scarp that tapers off in height from a maximum in the centre. The fault scarp has 125 m of relief at the centre.

We find no observable differences in the length of the fault traces between the two survey areas.

There is significant variation in the strike of fault segments imaged by sidescan sonar with increasing distance from the axis (Fig. 5). Consequently, we have subdivided the data into zones of increasing distance from the axis.

Comparison of the orientation data for successive pairs of zones using the *t*-test shows that the hypothesis that the two sets of data are drawn from the same population can be rejected at the 95% confidence level for the pairs 0–2 km and 2–4 km, and 2–4 km and 4–6 km, but cannot be rejected for the pairs 4–6 km and 6–10 km. The statistics for the fault segments in area C are shown in Table 1.

Over the first 2 kms from the axis the fault segments have a mean strike of 016.5°, sub-parallel both to the strike of the AVRs and to the spreading normal direction (Fig. 10). This is a very similar result to that found in area B over the same range, and indeed a *t*-test between this zone and the equivalent zone in area C shows them to have fault segment populations that are not significantly different. At 2–4 km from the axis the strike of the fault segments has changed in a clockwise sense by 3°, whereas the density of faults is the same. There is again no significant difference in the strike of fault segments between the 2–4 km zone and the equivalent zone within area B. The most dramatic change in the fault-segment distribution occurs at 4–6 km from the axis where the mean strike has rotated clockwise by 10°, to 029.5°, from that found in the previous area, and the density of faults has increased by 50% (Fig. 11). The increase in fault density at this distance from the axis coincides with faults measured from the bathymetry data, most of which were found at 5 km or greater from the axis. The strike of these faults is sub-parallel to the axis. At 6–10 km from the axis there is a reduction in the density of faults, with only a very slight shift in strike to 032°.

DISCUSSION

The data set presented above differs in some respects from recently published fault data from the same areas

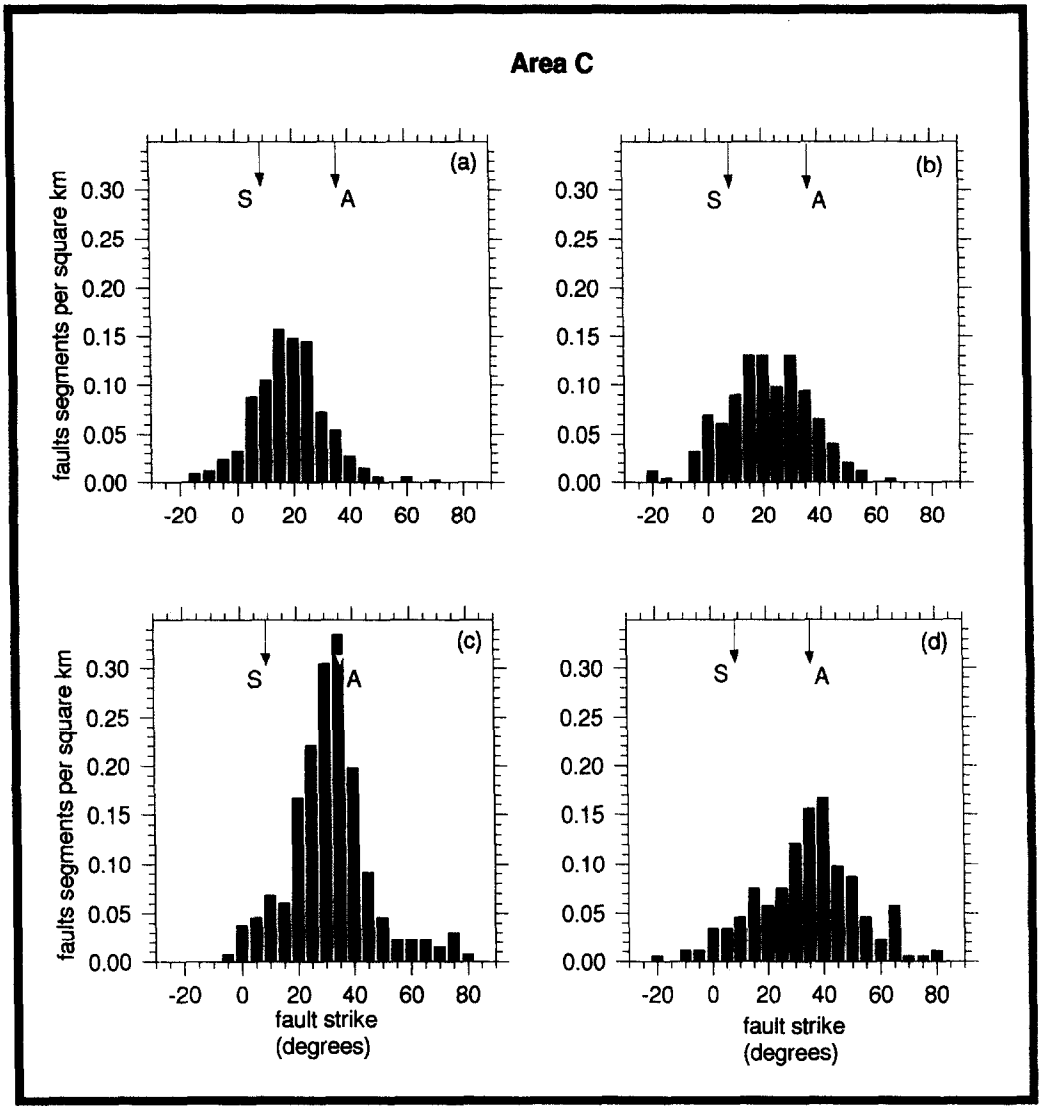

Fig. 10. Frequency diagrams showing the density of fault segments of a particular strike at incremental distances from the axis within area CC: (a) 0–2 km; (b) 2–4 km; (c) 4–6 km; and (d) 6–10 km. All the data has been normalized according to the percentage coverage of sidescan over the areas. The fault segments were all measured from the sidescan images, with each segment being 500 m in length.

of the Reykjanes Ridge (Murton & Parson 1993). Fault orientation in our data sets range between 330° and 084° (150°–264°), whereas Murton & Parson report fault orientations well outside our range. They argue for the existence of two families of transfer faults at a higher angle to the AVR trend than any faults seen by us. We have re-examined the original bathymetry, from which that of Fig. 4 from Murton & Parson (1993) was derived, in order to identify the regions where they record transfer faults. In all of the areas where Murton & Parson indicate a transfer fault we find no evidence to support their finding. Instead we would ascribe the features measured by them to two categories: (1) Some are artifacts introduced into the maps during the process of gridding across the gaps between bathymetric swaths. Such interpolations can make the edge of the ship track parallel swath prominent. Many of the faults reported by Murton & Parson run parallel to the ships track and fall into interpolated zones between swaths, where it would appear they have measured the edge of the swath as a transverse feature. (2) Other transverse features identified by Murton & Parson from the bathymetry maps as faults do not fulfil our criteria for faults, since they are not steep enough nor persistent enough. We consider these to be the ends of volcanic constructional features and/or mass wasting surfaces.

Broad-scale fault geometry

Despite the morphological contrasts between areas B and C, in both areas the broad-scale fault geometry, within the median valley, is the same. Both areas have an axial zone, running NE–SW parallel to the orientation of the ridge, 8–12 km wide. Within the axial zone there is an en échelon array of overlapping AVRs running nearly north–south. Associated with the AVRs are many small faults running nearly parallel to the AVR orientation and hence nearly perpendicular to the spreading direction. Mean fault orientation within the axial zone rotates clockwise towards a ridge-parallel trend as distance from the centre of the axial zone increases. This rotation of the mean fault orientation is

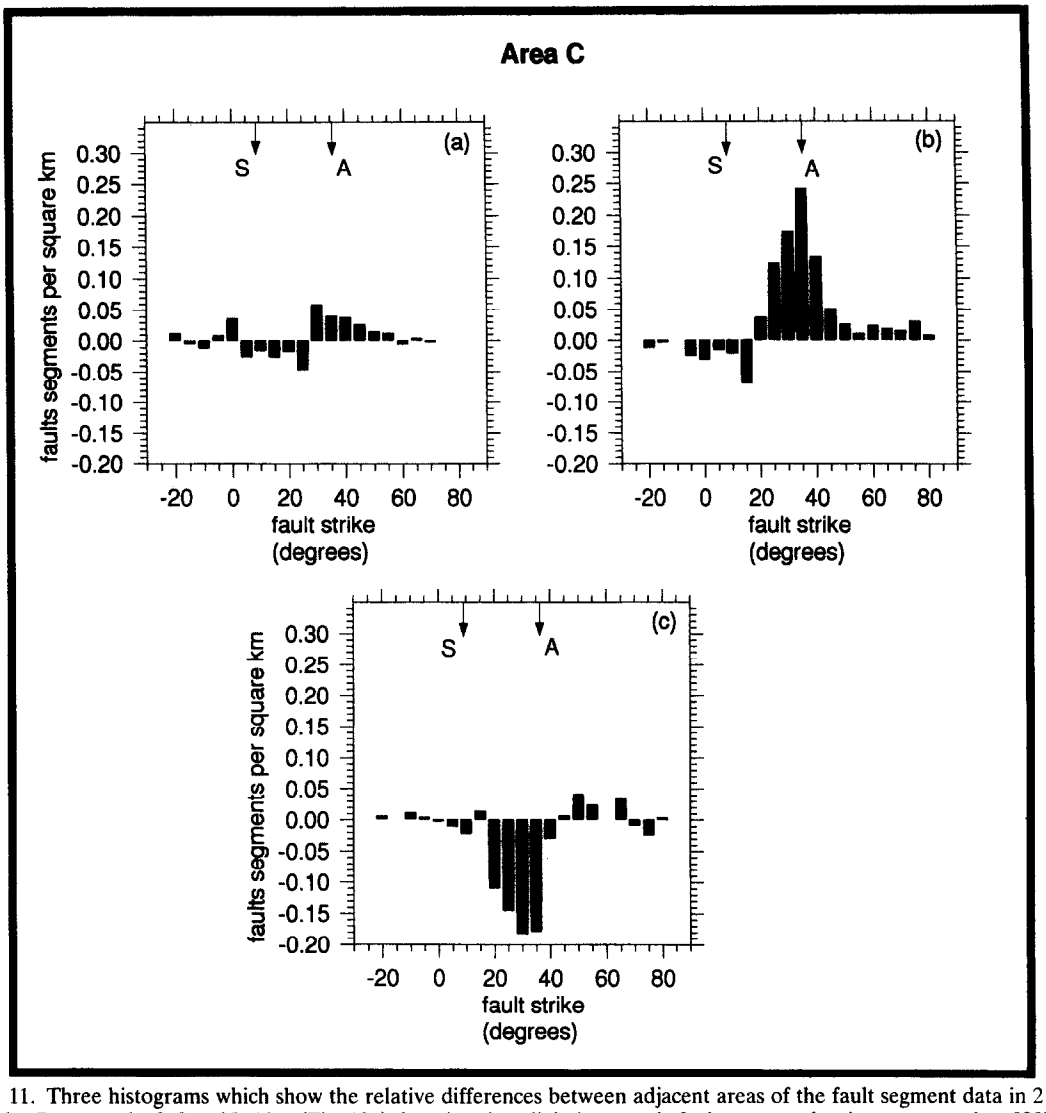

Fig. 11. Three histograms which show the relative differences between adjacent areas of the fault segment data in 2 km widths. Between the 0–2 and 2–4 km (Fig. 12a) there is only a slight increase in fault segment density at greater than 020°. A decrease in the number of AVR parallel faults with an increase in axis parallel faults occurs between 2–4 km and 4–6 km, while for the final two adjacent zones there is a decrease in the overall density pattern.

brought about by two factors; the covering of AVR-parallel faults near the centre of the axial zone by lava flows and by the initiation of new faults with a trend between AVR-parallel and ridge-parallel at a distance from the centre of the axial zone.

The margin of the axial zone is marked by major, ridge-parallel fault zones, spaced 5–10 km apart, which characterize the flanks of the ridge. Tectonic activity on each of these major fault zones is complete before the next one is generated. The variation in width of the axial zone and the spacing between major faults indicates that a new, major, fault is initiated on one side or other of the axial zone every 500,000 Ma. The overall fault geometry of the axial zone and the flanks is well seen on Fig. 12.

The AVRs within the axial zone are complex volcanic constructional features, tens of kilometres long, made up of numerous small volcanic edifices (Parson *et al.* 1993). The elongation of the AVRs must reflect the elongation of the underlying mantle flow structure and/or of the intra-crustal magmatic plumbing system (Murton & Parson, 1993). In either case, the AVRs represent extensional structures, with the direction of least compressive stress perpendicular to the orientation of the elongation of the AVRs and thus nearly east–west. This conclusion is consistent with the interpretation of the AVR-parallel faults of the axial zone as normal faults.

The overall geometry of the axial zone, with an en échelon array of extensional structures bounded by major linear faults, resembles closely the overall geometry of a major shear zone. Indeed Dauteuil & Brun (1993), interpreting a similarly en échelon segment of the Mohn's Ridge between Iceland and Svalbard, consider that the en échelon geometry results from a component of left-lateral strike-slip motion parallel to the ridge. Murton & Parson (1993) also recognized a strong similarity in fault patterns between the oblique rifting model (Dauteuil & Brun 1993) and the fault patterns along the Reykjanes Ridge though they reject a strike-slip model.

We consider this model to be mistaken. There are two observations that are inconsistent with it. First, close examination of the TOBI images of all faults, whether AVR parallel or ridge parallel, shows no sign of strike-slip motion. Individual volcanic features are displaced

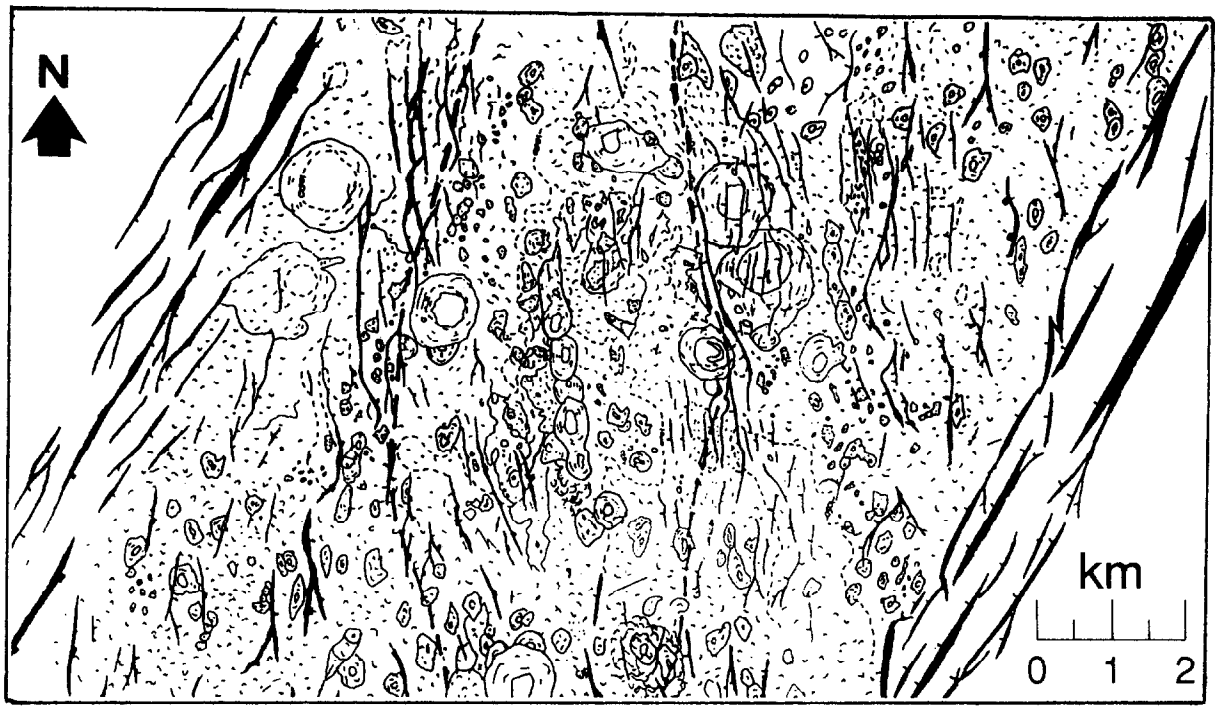

Fig. 12. Schematic drawing of an AVR bounded by obliquely oriented faults. Based on comparison between TOBI images and Hydrosweep maps of area C.

by dip-slip movement, and the focal mechanism, deduced from teleseismically recorded earthquakes on the Reykjanes Ridge, indicate normal faulting. Second, the local plate kinematics are well constrained, both by the orientation of nearby major transform faults such as Charlie–Gibbs fault at 52°N and by global analyses of plate motions (Minster & Jordan 1978). The integrated strain derived from plate kinematics is extension along an azimuth of 099° (Minster & Jordan 1978) approximately normal to the orientation of the AVRs. This means that an alternative model must be sought which is consistent with plate kinematics and with observed dip-slip fault displacements. Such a model must involve rotation of the stress field with distance from the spreading axis and hence with lithospheric age.

Faults in the centre of the axial zone

Faults in the centre of the axial zone run parallel to the trend of the AVRs which are oriented perpendicular to the spreading direction. These faults all have minor displacements at the surface, except at the latitude of the non-transform offset of Owens *et al.* (1991), but lie in a volcanically highly active environment, where construction of the AVRs is proceeding vigorously. The abundance and surface displacement of faults in such a situation depends on the relative rates of volcanic resurfacing and tectonic deformation. If faults in this area are continuously active then fault throw at the surface is not a true reflection of the tectonic contribution made by these faults, because of the repeated resurfacing. A fault with only a minor surface displacement may have considerable tectonic importance.

Without information from the sub-surface, it is not possible to evaluate the tectonic role of faults in this zone of active volcanic re-surfacing. For the same reason it is difficult to come to firm conclusions about the origin of these AVR-parallel faults. They may be tectonically fundamental, and result from the far-field plate stresses that generate the local plate movements, or they may be more superficial and result from local stresses such as those associated with dyke injection (Delaney *et al.* 1986, Pollard *et al.* 1982, Rubin & Pollard 1987, Rubin 1992) or gravitational forces acting on the AVRs. What we can conclude is that because of the orientation of the faults far-field plate stresses must have been important, if not dominant, in generating these faults. Also the close similarity between the fault populations of areas B and C within 4 km of the axis, implies that the Icelandic hotspot and the increased asthenospheric upwelling close to Iceland does not influence the stress field generated within the axial zone. Therefore a regional rather than local origin to the stress field is preferred.

Faults on the ridge flanks

Beyond the axial zone, further than 4 km from the spreading axis, new faults are generated, with a strike close to 035°, approximately axis-parallel. The pattern of this ridge flank faulting differs between areas B and C.

In area B, the fault segment density histogram (Fig. 7) shows a marked decrease in fault segment abundance between 2–4 and 4–6 km from the axis. This decrease is most marked for fault strike close to the spreading normal direction (036°). There is a small increase in fault segment density with axis parallel strike (036°). The major reduction in density reflects the covering of AVR-parallel faults by lava flows or sediments, indicating that by 4 km from the axis these faults have become inactive. A further decrease in AVR-parallel (spreading-normal)

fault segments occurs between 4–6 and 6–10 km from the axis. At this distance from the axis, the sidescan images are dominated by low backscatter which is attributed to attenuation of the sonar within the sediments (Mitchell 1993). Major axis-parallel faults were not imaged by bathymetric or sidescan surveys, but the GLORIA surveys of Searle & Laughton (1981) show that such faults do exist further from the axis at this latitude.

Area C, further from Iceland and in deeper water, shows similar features, but these are developed to different degrees. Between 2–4 and 4–6 km from the axis, there is a decrease in the density of fault segments with a strike close to AVR-parallel, but this decrease is much smaller than in area B. Conversely the increased number of fault segments striking ridge-parallel at the same distance from the axis is much greater than in area B. Within the band 4–6 km from the axis, abundant faults striking parallel to the ridge axis are generated and grow. These do not exploit the pre-existing faults and fractures generated parallel to the AVRs but must represent a new episode of crustal failure. Very few fault segments with a ridge-parallel strike are found closer than 4 km from the axis, corresponding to a crustal age of 400,000 years. Beyond 6 km from the axis, the abundance of these fault segments decreases again, as rapidly accumulating sediments covers them, indicating that at this stage the faults have already become inactive. Searle & Laughton (1981) showed on a larger scale that the throw of the second major faults from the axis, as imaged by the GLORIA long-range sidescan, is no different from that of the first major fault, indicating a narrow window in time and space for the growth of the axis-parallel faults.

In both areas B and C there is good evidence for the generation of a new family of ridge-parallel faults. In area C, generation starts close to 4 km from the axis and is complete at about 6 km from the axis. In area B, some faults of this new family are seen at about 4 km from the axis, but the major growth of these faults takes place further from the axis and outside the area imaged by Hydrosweep or TOBI. Those faults were, however, clearly imaged by GLORIA (Searle & Laughton 1981). Faults of this family have a mean strike of 035°, rotated 20° clockwise from the mean strike of the faults within the axial zone; the new family of faults does not exploit existing crustal faults. All indicators from the sidescan images are that the new family are dip-slip normal faults with no strike-slip motion. This implies a direction of least compressive stress oriented approximately 125–305°. Such a stress field is rotated considerably however, normal to the axis of the Reykjanes Ridge, indicating an origin related to ridge orientation. Searle & Laughton (1981) and Murton & Parson (1993) recognized this constraint, and suggested that the off-axis fault orientation is parallel to contours of equal lithospheric thickness, assuming a constant cooling rate for the lithosphere away from the ridge axis. We therefore tentatively suggest that stresses may be generated by thermal stresses, caused by lithospheric cooling or by gravitational effects of a thickening and cooling lithosphere. Whatever their precise origin, generation by stresses produced during lithospheric evolution seems necessary. The greater distance to the onset of these faults in area B we attribute to increased lithospheric temperatures resulting from thermal influences of the increased mantle upwelling associated with Iceland, with the elevated temperatures reducing the flexural rigidity of the lithosphere.

CONCLUSIONS

Detailed analysis of the tectonic structure of the Reykjanes Ridge has revealed a complex spatial and temporal evolution of the upper brittle crust. Within the axial zone, less then 4 km from the spreading axis, faults have a mean strike which is sub-parallel to the strike of the axial volcanic ridges. Most faults within this zone have vertical surface displacements, less than 50 m. There is no change in the character of faulting within this zone with increasing distance from Iceland. The family of faults within the axial zone are oriented normal to the plate-tectonic direction of least compressive stress and formed in a plate-tectonically generated regional stress field.

At the edge of the axial zone a new family of faults is generated with a strike close to the overall orientation of the Reykjanes Ridge, rotated about 20° clockwise from the fault strike within the axial zone. This new family of faults is most common in the survey area furthest away from Iceland, where generation and growth of the new faults is complete within 250,000–500,000 years. The faults have a greater mean throw than those in the axial zone. In the survey area near Iceland this family of faults is rare within 6 km of the axis.

The two different families of faults can be distinguished particularly clearly on the Reykjanes Ridge because it spreads obliquely. It is very likely that two successive generations of faults of different origin occur at other spreading centres where spreading is more nearly orthogonal to the ridge, and that two distinct processes are responsible for their growth there too. In an obliquely oriented spreading environment the overall spatial distribution of faulting has lead Dauteil & Brun (1993) to infer the presence of an oblique rifting dominated stress field. Our more detailed observations suggest, however, that this fault pattern is the product of two plate-tectonic generated stress fields of different origin acting in sequence.

Acknowledgements—The authors are indebted to their colleagues from the EW9008 cruise to the Reykjanes ridge, namely, P. Field, J. Keeton, A. S. Laughton, B. Murton, L. M. Parson, L. Redbourne, R. C. Searle, D. K. Smith, C. P. Summerhayes and C. Walker. The technical support staff and ships crew are also to be thanked. The authors have greatly benefited from discussions with members of the geology departments of Leeds and ETH. We would like to specifically thank C. Ebinger, R. Knipe and D. K. Smith for critical comments on early drafts. A thorough, constructive, review by A. Gudmundsson improved the final manuscript. We made extensive use of the GMT software of Wessel & Smith (1992) in displaying bathymetry and fault data. SS was funded by a Royal Society European Science Exchange Fellowship.

REFERENCES

Anderson, E. M. 1951. *The Dynamics of Faulting*. Oliver & Boyd, Edinburgh.

Bergman, E. A. & Solomon, S. C. 1990. Earthquake swarms on the Mid-Atlantic Ridge: products of magmatism or extensional tectonics? *J. geophys. Res.* **95**, 4943–4965.

Chen, Y. & Morgan, W. J. 1990. A non-linear rheology model for mid-ocean ridge axis topography. *J. geophys. Res.* **95**(B11), 17,583–17,604.

Dauteuil, O. & Brun, J.-P. 1993. Oblique rifting in a slow spreading ridge. *Nature* **361**, 145–148.

Delaney, P. T., Pollard, D. D., Ziony, J. J. & McKee, E. H. 1986. Field relations between dikes and joints: emplacement processes and paleostress analysis. *J. geophys. Res.* **91**, 4920–2938.

Flewellen, C., Millard, N. & Rouse, I. 1993. TOBI, a vehicle for deep ocean survey. *J. Elect. & Comm. Eng.* April, 85–93.

Gudmundsson, A. 1987. Geometry, formation and development of tectonic features of the Reykjanes Peninsula, south-west Iceland. *Tectonophysics* **139**, 295–308.

Hwang, C., Parsons, B., Strange, T. & Bingham, A. In press. A detailed Gravity field over the Reykjanes Ridge from Seasat, Geosat, ERS-1 and TOPEX/POSEIDON Altimeter Data and Shipbourne Gravity Data. *Geophys. Res. Lett.*

Jacoby, W. R. 1980. Morphology of the Reykjanes Ridge crest near 62N. *J. geophys.* **47**, 81–85.

Laughton, A. S., Searle, R. C. & Roberts, D. G. 1979. The Reykjanes Ridge crest and the transition between its rifted and non-rifted regions. *Tectonophysics* **55**, 173–177.

Macdonald, K. C. 1982. Mid-ocean ridges: fine scale tectonic, volcanic and hydrothermal processes within a plate boundary zone. *Annu. Rev. Earth & Planet. Sci.* **10**, 155–190.

Minster, J. B. & Jordan, T. H. 1978. Present-day plate motions. *J. geophys. Res.* **83**, 5331–5354.

Mitchell, N. C. 1993. A model for attenuation of backscatter due to sediment accumulations and its application to determine sediment thickness with GLORIA sidescan sonar. *J. geophys. Res.* **98**, 22,477–22,493.

Murton, B. J. & Parson, L. M. 1993. Segmentation, volcanism and deformation of oblique spreading centres: a quantitative study of the Reykjanes Ridge. *Tectonophysics* **222**, 237–257.

Owens, R. B., Searle, R. C. & Field, P. 1991. The first non-transfer offset on the Reykjanes Ridge. *EOS Abstracts* **72**, 467–477.

Parson, L. M., Murton, B. J., Searle, R. C., Booth, D., Evans, J., Field, P., Keeton, J., Laughton, A., McAllister, E., Millard, N., Redbourne, L., Rouse, I., Shor, A., Smith, D., Spencer, S., Summerhayes, C. & Walker, C. 1993. En échelon axial volcanic ridges at the Reykjanes Ridge: a life-cycle of volcanism and tectonics. *Earth Planet. Sci. Lett.* **117**, 73–87.

Pollard, D. D., Segall, P. & Delaney, P. T. 1982. Formation and interpretation of dilatant echelon cracks. *Bull. geol. Soc. Am.* **93**, 1291–1303.

Rubin, A. M. 1992. Dike-induced faulting and graben subsidence in volcanic rift-zones. *J. geophys. Res.* **97**, 1839–1858.

Rubin, A. M. & Pollard, D. D. 1988. Dike-induced faulting rift zones of Iceland and Afar. *Geology* **16**, 413–417.

Schilling, J. G. 1975. Rare-earth variations across 'normal segments' of the Reykjanes Ridge, 60°–55° N, Mid-Atlantic Ridge, 29°S, and East Pacific Rise 2°–19°S, and evidence of the composition of the underlying low-velocity layer. *J. geophys. Res.* **81**, 5294–5304.

Searle, R. C. & Laughton, A. S. 1981. Fine-scale study of tectonics and volcanics on the Reykjanes Ridge. Proc. 26th Int. Congress, Geology of oceans symposium, Paris. *Oceanologica Acta.* 5–13.

Sempere, J.-C. & Macdonald, K. C. 1987. Marine tectonics: processes at Mid-Ocean Ridges. *Rev. Geophys.* **25**, 1313–1347.

Sempere, J.-C., Purdy, G. M. & Schouten, H. 1992. Segmentation of the Mid-Atlantic Ridge between 24°00′N and 30°40′N. *Nature* **344**, 427–431.

Shih, J. S. F., Atwater, T. & McNutt, M. 1978. A near bottom geophysical traverse of the Reykjanes Ridge. *Earth Planet. Sci. Lett.* **39**, 75–83.

Smith, D. K. & Cann, J. R. 1992. The role of seamount volcanism in crustal construction at the Mid-Atlantic Ridge (24°–30°). *J. geophys. Res.* **97**, 1645–1658.

Talwani, M., Windisch, C. C. & Langseth, M. G. 1971. Reykjanes ridge crest: a detailed geophysical study. *J. Geophysics* **76**, 473–577.

Vogt, P. R. & Avery, O. E. 1974. Detailed magnetic surveys in the north-east Atlantic and Labrador sea. *J. geophys. Res.* **79**, 363–389.

Wessel, P. & Smith, W. H. 1991. Free software helps map and display data. *Eos Trans. Am. geophys. Un.* **72**, 441–446.